Journal of Materials Chemistry A

Modulating Reactivity and Stability of Metallic Lithium via Atomic Doping

Journal:	*Journal of Materials Chemistry A*
Manuscript ID	TA-ART-02-2020-002176.R1
Article Type:	Paper
Date Submitted by the Author:	26-Apr-2020
Complete List of Authors:	Lu, Ke; Northern Illinois University, Chemistry Xu, Haiping ; Northern Illinois University, Chemistry & Biochemistry He, Haiying; Valparaiso University, Department of Physics and Astronomy Gao, Siyuan; Northern Illinois University, Chemistry Li, Xun; Northern Illinois University, Chemistry and Biochemistry Chong, Zheng; Northern Illinois University, Chemistry and Biochemistry Xu, Tao; Northern Illinois University, Department of Chemistry and Biochemistry Cheng, Yingwen; Northern Illinois University College of Liberal Arts and Sciences, Chemistry and Biochemistry

Modulating Reactivity and Stability of Metallic Lithium *via* Atomic Doping

Ke Lu,[a] Haiping Xu,[a] Haiying He,[b] Siyuan Gao,[a] Xun Li,[a] Chong Zheng,[a] Tao Xu*,[a] and Yingwen Cheng*,[a]

[a] Department of Chemistry and Biochemistry, Northern Illinois University, DeKalb, Illinois, 60115, United States.

[b] Department of Physics and Astronomy, Valparaiso University, Valparaiso, Indiana, 46383, United States.

*E-mails: ycheng@niu.edu (Y.C.) and txu@niu.edu (T.X.)

TOC

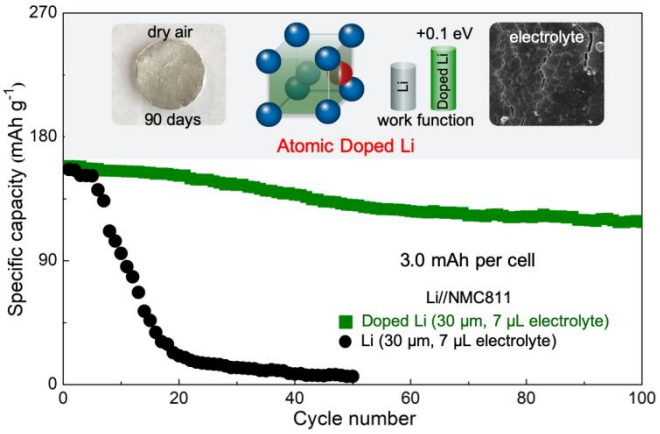
dry air
90 days
+0.1 eV
Li
Doped Li
work function
electrolyte
Atomic Doped Li
Specific capacity (mAh g-1)
270
180
90
0
0
20
40
60
80
100
Cycle number
3.0 mAh per cell
Li//NMC811
Doped Li (30 μm, 7 μL electrolyte)
Li (30 μm, 7 μL electrolyte)

Abstract:

Many approaches have been described to address challenges in metallic Li anodes but they rarely modulate its inherent chemical reactivities. Here we describe a general approach for modulating Li metal properties and enabling stable metal batteries by doping with ~ 0.1 at.% Ag or Al. The dopants were atomically dispersed in the vacant face-centered sites of the body-centered cubic Li crystals and pull electrons strongly due to higher electronegativity (Ag: 1.98; Al: 1.61 vs. Li: 0.98). As a result, the doped Li have increased work function with reduced chemical reactivity and remained shiny in dry air for months. They also exhibited enhanced Li^+/Li redox kinetics and generated thinner but stronger solid-electrolyte interphases in carbonate electrolytes. The dopant atoms are lithophilic and have stronger bindings with Li adatoms, which guide uniform Li deposition and ensures dendrite-free Li interface during battery cycling. Overall, the doped anodes enabled stable operations of not only high current symmetric cells but also practical full cells in which Ni-rich layered cathodes were paired with 30 μm anodes and 7 μL electrolytes. The doping approach is facile and scalable, and opens up new and promising opportunities for designing practical high energy density metal batteries.

Keywords: Doped Li metal; metal batteries; air stable Li; Li protection; directed deposition

Introduction

Lithium ion batteries designed with intercalation-type electrodes store electricity efficiently as chemical energy, and are extensively used in many areas including portable electronics, robotics and electric vehicles.[1, 2] However, they have limited energy densities (~ 150 Wh kg^{-1}) and are unable to cope with the growing cost and performance demands especially for the large-scale applications.[3-5] There are hence urgent needs for higher energy alternatives, and Li metal batteries that pair metallic Li anodes with high capacity cathodes such as sulfur, oxygen or Ni-rich oxides are among the most promising candidates.[6-8] The advantages of metallic Li anodes are now widely recognized, including ten times higher specific energy than graphite (3860 vs. 370 mAh g^{-1}), the lowest electrochemical potential (-3.040 V vs. SHE) and very low gravimetric density (0.59 g cm^{-3}).[9] The success of these candidates relies critically on the design of truly reversible lithium electrodes with stable electrode-electrolyte interfaces, as they are required for long lasting practical batteries with energy densities beyond 350 Wh kg^{-1} (lean electrolytes, low N/P ratio, no swelling, etc.).[10-13]

The extremely high reactivity of Li metal poses several critical challenges that are currently roadblocking its commercialization.[14, 15] Li spontaneously react with almost all liquid electrolytes and form fragile solid-electrolyte interfaces (SEI), which irreversibly consume both Li metal and electrolytes during battery cycling.[16, 17] In addition, these SEI layers induce turbulences in local Li-ion flux and accelerate growth of unsafe dendrite.[18 19] Many approaches have been demonstrated to stabilize Li metal during battery cycling. Specifically, a variety of integrated Li anodes were fabricated by infusing Li in 3D structural hosts such as porous carbon, graphene, metallic and polymeric foams and exhibited improved stability, largely due to significantly reduced effective current densities.[20-23] These hosts can be further modified via

heteroatoms or lithophilic nanoparticles, which improve Li wetting and smooth Li surface during dynamic cycling.[24-26] The coating of Li metal with artificial protection films, using materials such as Li-alloys, graphene, metal fluorides and nitrides, is another approach for improving Li stability. These films shielded reactive Li metal from liquid electrolytes, and extended electrode life by reducing detrimental side reactions.[27-31] Additionally, more stable Li cycling was described using novel electrolytes and additives that promote formation of stronger SEI layers, such as concentrated ether electrolytes, fluorinated electrolytes and dual salts electrolytes.[12, 32-37] In general, although these approaches assist fabrication of Li metal electrodes with improved stability, they are unable to modulate the inherent physicochemical properties of metallic Li and therefore the performance improvements are fundamentally limited. It is therefore of great interests and practical significance to explore approaches specifically designed to manipulate the fundamental behavior of Li metal.

Li-rich intermetallic alloys with the general formula of Li_xM (M = Si, Sn, Al or Mg) have attracted significant interests as alternative anodes for Li metal batteries.[38-40] Lithium in these alloys generally have lower chemical activity and modified surface properties, which reduce formation of dendritic structures and improve high-current performance. However, almost all of these alloys contained large amounts of alloying elements (> 10%) and therefore their energy density is smaller than pure Li. In addition, these alloys can only survive limited cycles due to the large volume changes during cycling and formation of unstable nanoporous sponge structures during Li stripping.[29, 30, 41, 42] On the other hand, the application of trace level dopant is a powerful approach to alter the electrical or optical properties of a substrate and provides materials that revolutionized fields such as solid-state electronics and lasers.[43, 44] We examined this approach to Li metal and report herein that the doping with 0.1 at. % Ag or Al produced Li

electrodes with significantly reduced chemical reactivity and very stable cycling. The dopant atoms are atomically dispersed and reside at the otherwise vacant face-centered sites within the body-centered cubic (BCC) structure of Li crystal. The dopants have higher electronegativity than Li atoms and strongly attract electrons in their vicinity, which increases the work function and reduces the reactivity of Li metal, leading to doped electrodes that are surprisingly stable in dry air for months. Importantly, the doped electrode exhibited higher Li^+/Li redox kinetics and significantly improved the fast charging capability of Li metal batteries. We further show that the dopant atoms have stronger binding with Li adatoms and guide uniform Li plating, which fundamentally mitigate growth of notorious unsafe dendrites. The combination of these benefits promoted generation of much thinner but stronger SEI layers during cycling in carbonate electrolytes, and enabled high-capacity and dendrite free battery cycling both in symmetric cells and in realistic full cells.

Results and Discussion

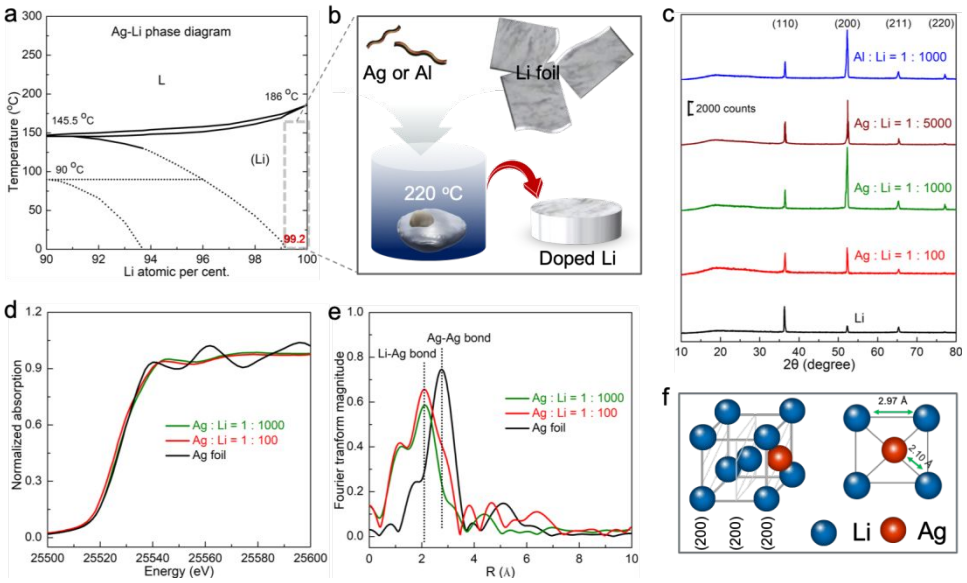

Figure 1: Synthesis and structural characterization of doped Li metals: a) Li-Ag phase diagram that rationalizes uniform dispersion of Ag atoms upon cooling the molten mixtures when Ag molar concentrations are < 1%; b) illustration of the synthesis process; c) XRD patterns of pristine and doped Li with different molar ratios. The doping noticeably enhanced the intensity of (200) peak; d) XANES and e)

EXAFS spectra of Ag K-edge in doped Li electrodes. The spectra from Ag foils are included for comparison; f) the structural characterizations identify dopant atoms reside the face-centered sites in BCC Li crystal structure.

We focused on Ag as the dopant since it has similar atomic radius as Li (1.65 vs. 1.67 Å for Li). Its atomic concentration was varied from 0.02% to 1% to ensure complete solvation without formation of crystalline compounds, which was determined from the Li-Ag phase diagrams (Figure 1a).[45] The doped Li metal samples were prepared inside an Ar-filled glovebox. Typically, 2.0 g Li was loaded in a crucible and was melted at 220ºC. A piece of silver wire was then introduced and it usually dissolve in molten Li within a few seconds (Figure 1b).[46] The mixture was kept at 220ºC for 2 hours to ensure complete homogenization, and was cooled afterward naturally. A piece of solidified Li lump was obtained (Figure S1), which was pressed to foils after cutting off the surface layers with a razor blade for battery assembly and testing. The undoped Li electrodes were prepared using the same melting-cooling procedure to ensure appropriate comparison. In addition to Ag, Li metals doped with Al were also prepared and studied. All the produced Li electrodes had grain sizes ~ 45 nm and likely had similar microstructure. No measurable differences in electrochemical properties were observed for Li electrodes with and without the melting-quenching procedure.

The X-ray diffraction (XRD) patterns of the doped Li metals exhibited peaks that can be indexed exclusively to the BCC structure of metallic Li (Im-3m, Figure 1c) and no crystalline intermetallic compounds were identified. Notably, the doped samples exhibited dramatically enhanced intensity for the (200) diffraction peak. Figure 1d-e compare the K-edge X-ray absorption near-edge structure (XANES) and extended X-ray absorption fine structure (EXAFS) spectra of Ag in doped Li and pure Ag foils. The XANES spectra of Ag in doped Li are distinctly different from Ag foils and confirm the complete solvation in metallic Li. In addition,

the Ag energy in Ag-doped Li appears more negative than Ag foil, suggesting shift of electron density due to the greater electronegativity (Ag: 1.98 vs. Li: 0.98). Meanwhile, the FT k3-weighted oscillation curves in EXAFS suggest the average bonding distance between Ag and Li in R space was ~ 2.1 Å, which corresponds to 2.5 Å after phase shift, and no signatures corresponding to Ag-Ag bonding were observed. Importantly, the correlation of enhanced (200) peak in XRD and the 2.5 Å Ag-Li bonding distance reveals that the Ag dopants occupied the otherwise vacant face-centered sites in Li crystals as shown schematically in Figure 1f. Furthermore, this assignment is also supported by density functional theory (DFT) calculations and the formation energy of positioning Ag atoms at interstitial face-centered site is favored compared with substitutional sites (-2.27 vs. -1.47 eV, Figure S2). The rationales for such assignment and how this enhance the (200) peak are detailed in the supplemental information. On the other hand, preferred crystallographic orientation could also contribute to the enhancement in (200) peak. We note that this does not seems as a major contributing factor as similar results were obtained regardless how the Li lumps were rolled and preferred orientation alone unlikely generate such pronounced increases in diffraction peaks.

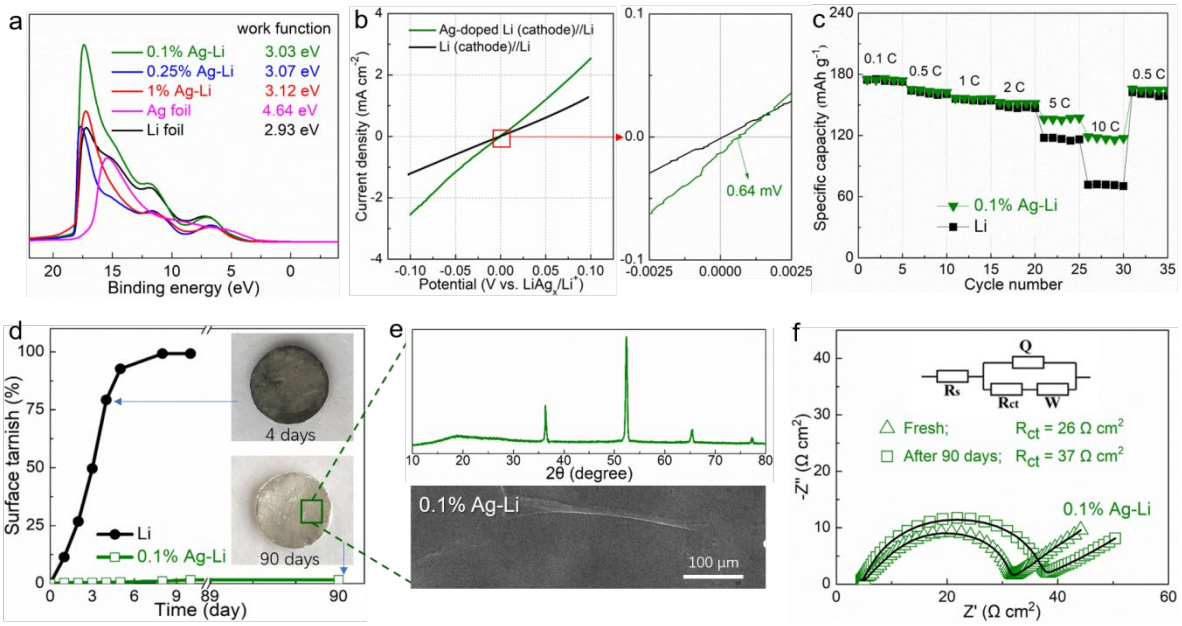

Figure 2: The doped Li metal has reduced chemical reactivity and enhanced electrochemical activity: a) UPS spectra and estimated work functions of Li doped with various level of Ag, the results of Li foil and Ag foil are included for comparison; b) Comparison of LSV polarization curves acquired from coin cells assembled with either Ag-doped Li or undoped Li as the cathode and undoped Li as the anode; c) rate capability of full cells assembled with NMC 811 cathode and either Ag-doped or undoped Li anodes; d) surface tarnishing of pristine and doped Li electrodes in dry air; e) XRD/SEM results and f) Nyquist plots of Ag-doped Li electrodes before and after 90 days of exposure in dry air.

The doped Li metals have reduced chemical reactivity and significantly improved dry air stability. The Ag dopants modulate charge distribution in Li metals due to higher electron negativity as revealed by DFT studies of Li (100) model surface (Figure S3). DFT also suggests that the work function of Ag-doped surface (Ag:Li = 1:128) increased to 3.11 eV from the 3.05 eV of undoped Li, which was also quantified by Ultraviolet Photoelectron Spectroscopy (UPS) as by 0.1~0.2 eV after Ag doping (Figure 2a)and confirming reduced reactivity of surface electrons. On the other hand, the impacts of dopants on interfacial charge transport and the Li^+/Li redox couple was examined in the 1.0 M $LiPF_6$ in EC/DEC electrolyte using coin cells assembled with an either Ag-doped Li or undoped Li as the cathode and an undoped Li electrode with twice surface area as the anode. The cell with the doped electrodes exhibited linear

polarization curves without abnormal redox peaks but with notably higher slopes (Figure 2b), suggesting enhanced interfacial redox kinetics. The $Li^+/LiAg_x$ couple exhibited a slightly higher redox potential and positively shifted ~ 0.64 mV compared with Li^+/Li as a result of increases in work function. Furthermore, the electrochemical impedance spectroscopy (EIS) analysis revealed that all of the doped electrodes have lower charge-transfer resistance (R_{ct}) and higher Li^+ ions diffusion coefficient (D_{Li+}) compared with undoped Li not only in carbonate but also in ether electrolytes (Figure S4), suggesting intrinsically promoted redox kinetics. The 0.1 at.% Ag doped Li metal has the best combination of properties and was therefore studied in more detail (referred as Ag-Li hereafter). As expected, the fast charging Ag-Li electrodes enabled Li metal batteries with notably improved high rate performance. Figure 2c presents that full cells assembled with NMC 811 cathodes and Ag-Li anode delivered a high capacity retention of 65% as the rate was increased from 0.1C to 10C, as opposed to the 42% for the undoped Li based full cells.

We then compared the dry air stability of Ag-Li and undoped Li electrodes under relative humidity <5%. The undoped Li exhibited typical aggressive reactivity and formed characteristic tarnishing layers composed of Li_3N and Li_2O almost immediately (Figure 2d, S5).[47] The doped Li, in strong contrast, had outstanding stability and remained shiny for months without generating noticeable tarnishing layers. The surface of doped Li remained flat and dense whereas pristine Li become very porous with abundant corrosion pits (Figure 2e). Further surface analysis using XPS revealed that the doped electrodes developed thin surface layers with notably less amounts of Li_2O and Li_2CO_3, and almost no Li_3N was observed. The Ag 3d XPS spectrum suggests a portion of the Ag dopant was oxidized, which likely played key roles in stabilizing the surface (Figure S6). In addition, we studied the impacts of surface tarnishing on the

electrochemical activity by performing EIS analysis of symmetric coin cells assembled with doped Li electrodes after different days of exposure (Figure 2f). The results suggest that the R_{ct} of Ag doped Li electrodes only increased slightly after 90 days of exposure (26 to 37 Ω cm^2), which is dramatically better than the more than 20 increases of pristine Li electrodes within only two days (Figure S5). These results imply intrinsic dry-air stability of Li metal as a result of Ag doping, which can enable their direct integrations in the dry room based industrial manufacturing facilities without costly surface protection treatments.

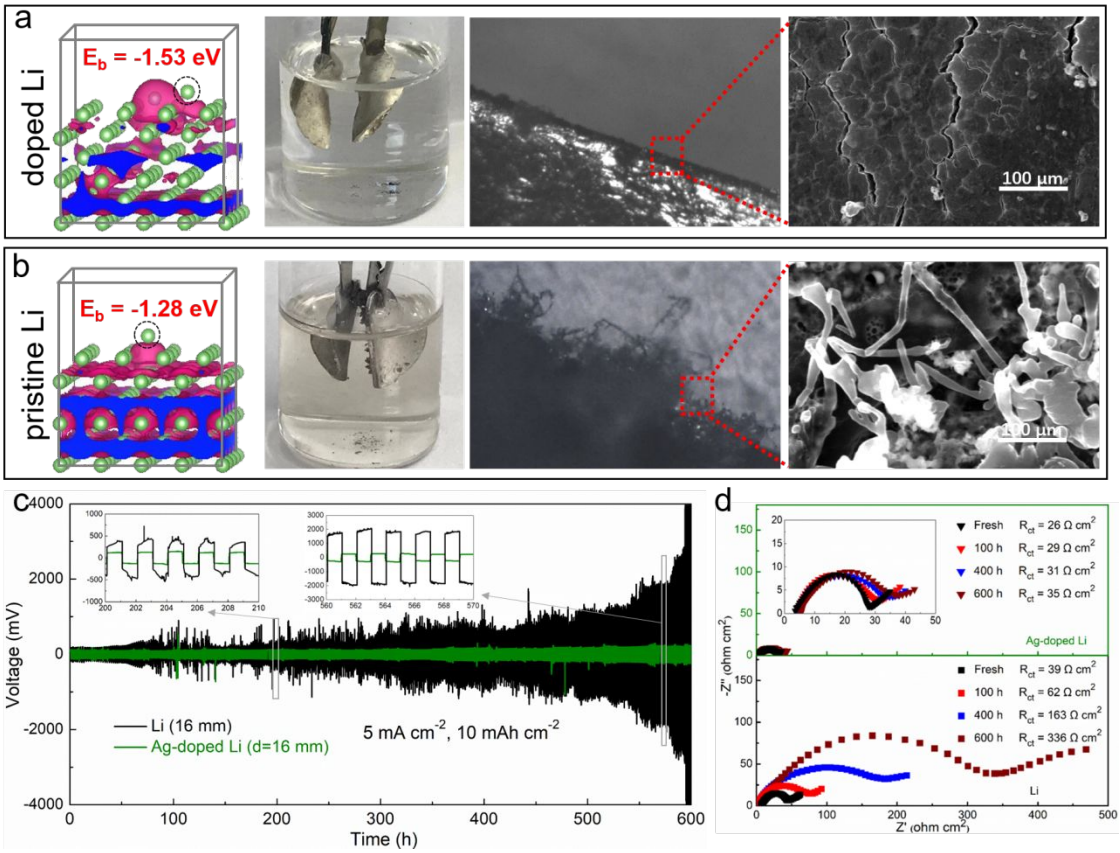

Figure 3: Ag doped Li metal electrodes have improved stability and dendrite-free Li plating in carbonate electrolytes: comparisons of a) Ag doped Li and b) pristine Li electrodes for Li plating, including DFT calculation that shows favorable binding energies (E_b) for positioning Li adatoms near Ag dopants on Li (100) surface (charge density isosurface value set to = 0.0080 e/Å^3) and photographs/SEM images that visualize smooth electrolyte-electrode interface during dynamic Li deposition; c) Voltage profiles of coin cells of symmetric pristine or Ag doped Li electrodes cycled at 5 mA cm^{-2} for a capacity of 10 mAh cm^{-2} per cycle; d) Nyquist plot of symmetric cells after different cycles;

The Ag-Li electrodes have significantly improved stability and enabled dendrite-free Li plating in carbonate electrolytes. DFT studies of the energetics of Li plating on the model Li (100) surface suggest that the binding of Li adatoms on Ag-doped Li surface was notable stronger (-1.53 vs. -1.28 eV of the undoped surface, Figure 3a-b). In addition, the binding of Li adatom at sites closer to Ag dopants were always stronger, which implies Ag atoms are lithiophilic and capable of direct Li deposition for maintaining smoother surface. This was further verified by examinations of Li metal-electrolyte interfaces during Li plating using a custom-built optical cell and a beaker cell (Figures 3a,b, and S7). The photographs captured using an optical microscope suggest that Li deposited on Ag-doped Li electrodes remained smooth and shiny whereas substantial dendrites were observed on pristine Li electrodes at the early stages of deposition, similar results were obtained with ex-situ SEM images. Furthermore, the stability was also evaluated using coin cells assembled with symmetric 2.0 cm^2 electrodes. The Ag doped Li anodes have outstanding stability even an aggressive current density of 5 mA cm^{-2} and a high capacity of 10 mAh cm^{-2} per cycle (Figure 3c). The overpotentials associated with Li stripping/stripping remained relatively flat throughout the 600 hours testing, suggesting uniform Li plating without substantial perturbance in surface architectures. Although some random abnormal voltage spikes were indeed observed, such phenomenon was mostly associated with depletion of surface Li-ions under high currents and was generally disappeared shortly. The undoped Li anodes, in strong contrast, exhibited substantial voltage fluctuations with large spikes for almost all cycles, which are characteristic of growing both mossy dendrites and the unsafe spike dendrites. In addition, the cell also exhibited failures due to consumption of electrolytes after ~ 450 hrs, further confirming the unstable nature of pure Li-electrolyte interface.[48] The Nyquist plots acquired during cycling also confirm stable electrode-electrolyte interface for Ag-

doped electrodes, as the increases in R_{ct} during cycling were substantially smaller (Figure 3d). The testing at 4.0 mA cm^{-2} reveal similar and consistent results (Figure S8). Additionally, the doped electrodes exhibited consistently smaller overpotentials for all current densities examined (1~5 mA cm^{-2}), which are consistent with improved high-current performance as discussed above (Figure S9).

Figure 4 demonstrates Ag-doped Li anodes substantially extended the cycle life of full cells paired with high loading NMC 811 cathodes (3.0 mAh per cell). These cells were primary evaluated using thin Li foils (30 and 80 μm) and lean electrolytes, as such conditions are required for practical batteries with specific energies exceed 350 Wh kg^{-1}.[21, 49] As expected, the Ag-Li||NMC 811 cells equipped with 30 μm Li foils (corresponds to a N/P ratio of 4.1 and 230% excess Li) and 7 μL electrolyte exhibited stable cycling. The capacity retention was 74.5% for 100 cycles at 1.0 C and the Coulombic efficiency (CE) was maintained at nearly unity (Figure 4a, S10). Meanwhile, the voltage profiles were relatively stable and did not show significant increase in overpotential during cycling (Figure 4b). Importantly, cells assembled with the slightly thicker 80 μm Ag-Li foils and the conventional 400 μm foils exhibited stabilities that are essentially identical, further highlighting the remarkable interfacial stability between doped anode and carbonate electrolyte (Figure S11). These stabilities were in sharp contrast with thin undoped Li electrodes under lean conditions, where premature failure was commonly observed within only 20 cycles due to rapid Li degradation and electrolyte depletion.[21]

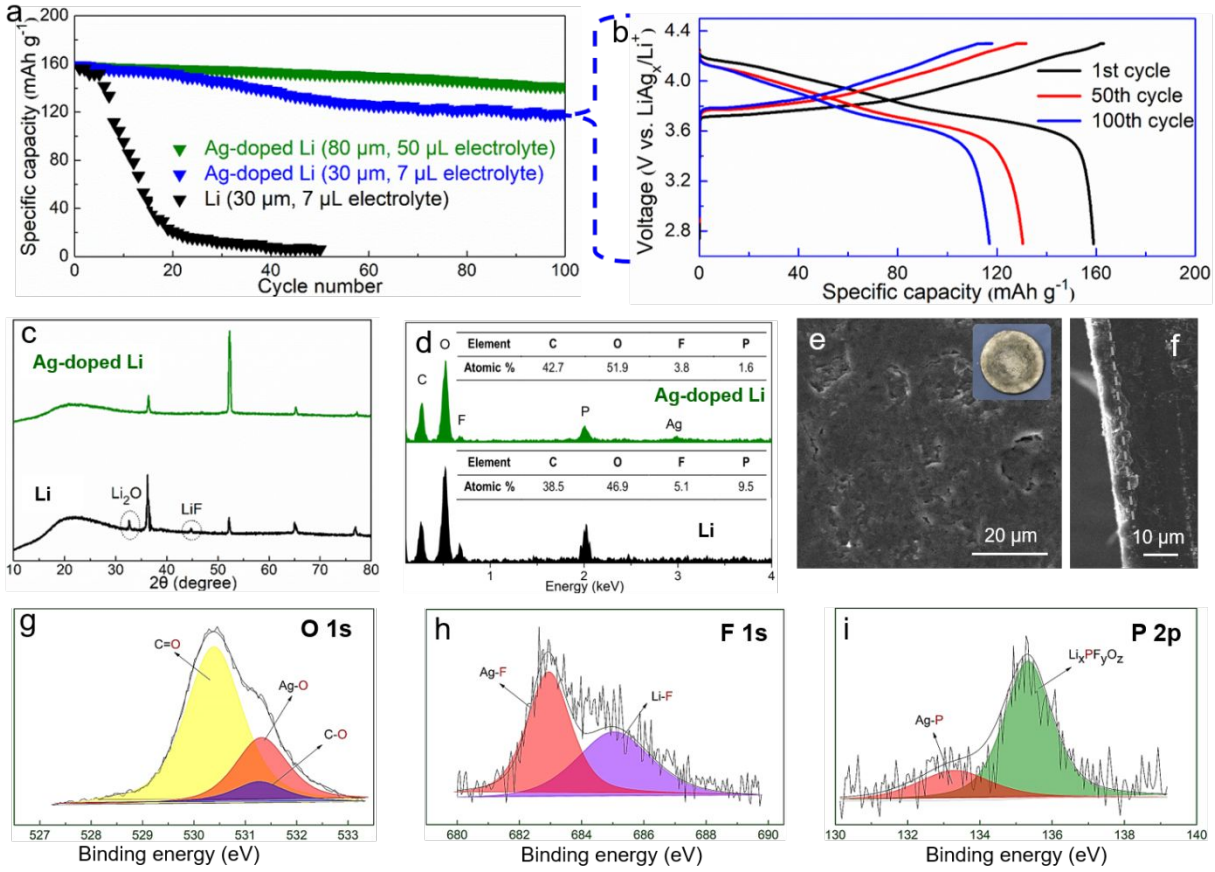

Figure 4: Doped Li anodes enable stable cycling of full cells incorporating NMC 811 cathode: a) cycling profiles of cells equipped with doped or pristine Li electrodes and different amount of electrolyte as specified (rate=1C). The cell with ~ 30 μm doped anode and 7 μL electrolyte exhibited outstanding stability and its voltage profile at the 1st, 50th and 100th cycle is compared in b. Characterization of Li metal anodes after 200 cycles: c) XRD patterns and d) EDS spectra of doped and pristine Li electrodes; e-f) SEM images and g-i) high resolution XPS spectra for Ag-doped Li electrodes.

Figure 4c-i present a series of post-mortem analysis of deeply cycled Li metal electrodes. The XRD patterns of Ag-Li anodes only exhibited diffraction peaks from crystalline Li (Figure 4c), as opposed to the strong Li_2O and LiF peaks from pristine Li electrode. Although in principle the Ag dopants should progressively concentrate during cycling and convert to some Ag-rich alloy phases, such phases were not detected perhaps due to small quantity and/or amorphous crystallinity nature. The energy-dispersive X-ray spectroscopy (EDS) analysis reveals that the contents of F and P in the SEI layers generated on Ag-Li electrodes were both

much lower compared with pristine Li electrodes (Figure 4d). Furthermore, the Ag-Li electrodes generated SEI layers that have flat morphology and much thinner (Figure 4e-f), suggesting reduced electrolyte decomposition that is critical for stable operation under lean conditions. The SEI layers appeared to be very dense without porous structure and adhere to the underlying metallic Li strongly, which agrees with the stable R_{ct} and lower ESCA as discussed above. The chemical composition and binding information of these SEI layers were further analyzed using X-ray photoelectron spectroscopy (XPS, Figure 4g-I, S12-13). Both doped and pristine Li electrodes show dominance of carbonyl groups (C=O) and ether oxygen (C-O) in O 1s and C 1s spectra, suggesting decomposition of carbonate solvents during cycling. The SEI generated on pure Li contains significant quantity of lithium oxides, but such species were not detected in the SEI generated on doped Li and the oxide species can be best attributed to the Ag-O groups. The F 1s and P 2p spectra both reveal formation of AgF and AgP_x compounds, respectively. The formation of such silver compounds likely contributed to robust SEI in addition to the better chemical stability as a result of Ag doping. Additionally, the Ag 3d spectra only show peaks from ionic silver species and no Ag^0 signal was observed (Figure S13). The combination of these beneficial effects reduced depletion of electrolyte and slows Li corrosion, leading to significantly enhanced stability under thin Li foils and lean electrolytes.

Conclusion

In summary, we demonstrated that the application of atomic doping with Ag or Al effectively modulates the chemical reactivities of metallic Li and lead to designable Li electrodes with favorable properties for Li metal batteries. We identified that the dopant atoms selectively occupy the vacant face centered sites in the body centered cubic structure of Li crystals. The dopant has higher electronegativity compared with Li and strongly attract electrons in their

vicinity, which increase the work function and makes Li metal more inert toward reacting with air and electrolyte. The doped Li electrodes delivered higher Li^+/Li redox kinetics with lower charger transfer resistance that are desired for high-power Li metal batteries. As a result of promoted redox activity and improved stability, these doped Li electrodes exhibited significantly improved stability in both symmetric cells and Li metal batteries coupled with NMC 811 cathodes. Our approach is facile and could be readily scaled up, and provides a viable approach to achieve practical Li metal anode especially when combined with the recent development in advanced electrolytes. The doping fundamentally alters the electrochemical behavior of Li, and allows the access of its physicochemical properties that are unlikely unattainable with traditional approaches, which opens up new and promising opportunities for the design of practical Li metal batteries.

Competing interests

The authors declare no competing financial interests.

Acknowledgements

This work was supported by startup funds provided to Y.C. from Northern Illinois University. Use of the Center for Nanoscale Materials, an Office of Science user facility, was supported by the U.S. Department of Energy, Office of Science, Office of Basic Energy Sciences, under Contract No. DE-AC02-06CH11357. This research used resources of the Advanced Photon Source, a U.S. Department of Energy (DOE) Office of Science User Facility operated for the DOE Office of Science by Argonne National Laboratory. The NMC cathodes were produced at the U.S. Department of Energy's (DOE) CAMP (Cell Analysis, Modeling and Prototyping) Facility, Argonne National Laboratory. The CAMP Facility is fully supported by the DOE

Vehicle Technologies Program (VTP) with the core funding of the Applied Battery Research (ABR) for Transportation Program.

Supplemental Information

Complete experimental details, computational methods, additional structural and electrochemical analysis. Figure S1-16 that include supplemental electrochemistry results, photographs and SEM images of electrodes and spectroscopy results.

References:

1. M. S. Whittingham, *Chemical Reviews*, 2014, **114**, 11414-11443.
2. K. Yan, J. Wang, S. Zhao, D. Zhou, B. Sun, Y. Cui and G. Wang, *Angewandte Chemie*, 2019, **131**, 11486-11490.
3. Z. Yang, J. Zhang, M. C. W. Kintner-Meyer, X. Lu, D. Choi, J. P. Lemmon and J. Liu, *Chemical Reviews*, 2011, **111**, 3577-3613.
4. B. Scrosati, J. Hassoun and Y.-K. Sun, *Energy & Environmental Science*, 2011, **4**, 3287-3295.
5. Z. Jiang, L. Jin, Z. Han, W. Hu, Z. Zeng, Y. Sun and J. Xie, *Angewandte Chemie International Edition*, 2019, **58**, 11374-11378.
6. K. Lu, H. Zhang, S. Gao, H. Ma, J. Chen and Y. Cheng, *Advanced Functional Materials*, 2018, **0**, 1807309.
7. P. Albertus, S. Babinec, S. Litzelman and A. Newman, *Nature Energy*, 2018, **3**, 16-21.
8. D. Lin, Y. Liu and Y. Cui, *Nature Nanotechnology*, 2017, **12**, 194.
9. W. Xu, J. Wang, F. Ding, X. Chen, E. Nasybulin, Y. Zhang and J.-G. Zhang, *Energy & Environmental Science*, 2014, **7**, 513-537.
10. X.-B. Cheng, R. Zhang, C.-Z. Zhao and Q. Zhang, *Chemical Reviews*, 2017, **117**, 10403-10473.
11. J. Qian, W. A. Henderson, W. Xu, P. Bhattacharya, M. Engelhard, O. Borodin and J.-G. Zhang, *Nature Communications*, 2015, **6**, 6362.
12. J. Zheng, M. H. Engelhard, D. Mei, S. Jiao, B. J. Polzin, J.-G. Zhang and W. Xu, *Nature Energy*, 2017, **2**, 17012.
13. J. Liu, Z. Bao, Y. Cui, E. J. Dufek, J. B. Goodenough, P. Khalifah, Q. Li, B. Y. Liaw, P. Liu, A. Manthiram, Y. S. Meng, V. R. Subramanian, M. F. Toney, V. V. Viswanathan, M. S. Whittingham, J. Xiao, W. Xu, J. Yang, X.-Q. Yang and J.-G. Zhang, *Nature Energy*, 2019, **4**, 180-186.
14. M. D. Tikekar, S. Choudhury, Z. Tu and L. A. Archer, *Nature Energy*, 2016, **1**.
15. D. Aurbach, E. Zinigrad, Y. Cohen and H. Teller, *Solid State Ionics*, 2002, **148**, 405-416.
16. G. Bieker, M. Winter and P. Bieker, *Physical Chemistry Chemical Physics*, 2015, **17**, 8670-8679.
17. Y. Li, Y. Li, A. Pei, K. Yan, Y. Sun, C.-L. Wu, L.-M. Joubert, R. Chin, A. L. Koh, Y. Yu, J. Perrino, B. Butz, S. Chu and Y. Cui, *Science*, 2017, **358**, 506.

18. D. Lu, Y. Shao, T. Lozano, W. D. Bennett, G. L. Graff, B. Polzin, J. Zhang, M. H. Engelhard, N. T. Saenz, W. A. Henderson, P. Bhattacharya, J. Liu and J. Xiao, *Advanced Energy Materials*, 2014, **5**, 1400993.
19. D. Aurbach, E. Zinigrad, H. Teller and P. Dan, 2000, **147**, 1274-1279.
20. G. Li, Z. Liu, Q. Huang, Y. Gao, M. Regula, D. Wang, L.-Q. Chen and D. Wang, *Nature Energy*, 2018, **3**, 1076-1083.
21. C. Niu, H. Pan, W. Xu, J. Xiao, J.-G. Zhang, L. Luo, C. Wang, D. Mei, J. Meng, X. Wang, Z. Liu, L. Mai and J. Liu, *Nature Nanotechnology*, 2019, **14**, 594-601.
22. J. Zhao, G. Zhou, K. Yan, J. Xie, Y. Li, L. Liao, Y. Jin, K. Liu, P.-C. Hsu, J. Wang, H.-M. Cheng and Y. Cui, *Nature Nanotechnology*, 2017, **12**, 993.
23. K. Li, Z. Hu, J. Ma, S. Chen, D. Mu and J. Zhang, *Advanced Materials*, 2019, 1902399.
24. Y. Chunpeng, Y. Yonggang, H. Shuaiming, X. Hua, H. Emily and H. Liangbing, *Advanced Materials*, 2017, **29**, 1702714.
25. W. Shuilin, Z. Zhenyu, L. Minhuan, Y. Shaoran, C. Junye, C. Junjie, S. Jianhua, Z. Ying, Z. Kaili and Z. Wenjun, *Advanced Materials*, 2018, **30**, 1705830.
26. R. Zhang, X.-R. Chen, X. Chen, X.-B. Cheng, X.-Q. Zhang, C. Yan and Q. Zhang, *Angewandte Chemie International Edition*, 2017, **56**, 7764-7768.
27. Y. Gao, Y. Zhao, Y. C. Li, Q. Huang, T. E. Mallouk and D. Wang, *J Am Chem Soc*, 2017, **139**, 15288-15291.
28. J. Zhao, L. Liao, F. Shi, T. Lei, G. Chen, A. Pei, J. Sun, K. Yan, G. Zhou, J. Xie, C. Liu, Y. Li, Z. Liang, Z. Bao and Y. Cui, *J Am Chem Soc*, 2017, **139**, 11550-11558.
29. X. Liang, Q. Pang, I. R. Kochetkov, M. S. Sempere, H. Huang, X. Sun and L. F. Nazar, *Nature Energy*, 2017, **2**.
30. Z. Tu, S. Choudhury, M. J. Zachman, S. Wei, K. Zhang, L. F. Kourkoutis and L. A. Archer, *Nature Energy*, 2018, **3**, 310-316.
31. K. Lu, S. Gao, R. J. Dick, Z. Sattar and Y. Cheng, *Journal of Materials Chemistry A*, 2019, **7**, 6038-6044.
32. S. Wei, S. Choudhury, Z. Tu, K. Zhang and L. A. Archer, *Accounts of Chemical Research*, 2018, **51**, 80-88.
33. S. Xin, Y. You, S. Wang, H.-C. Gao, Y.-X. Yin and Y.-G. Guo, *ACS Energy Letters*, 2017, **2**, 1385-1394.
34. N. W. Li, Y. X. Yin, C. P. Yang and Y. G. Guo, *Adv Mater*, 2016, **28**, 1853-1858.
35. J. Liang, X. Li, Y. Zhao, L. V. Goncharova, G. Wang, K. R. Adair, C. Wang, R. Li, Y. Zhu, Y. Qian, L. Zhang, R. Yang, S. Lu and X. Sun, *Adv Mater*, 2018, DOI: 10.1002/adma.201804684, e1804684.
36. M. S. Kim, J.-H. Ryu, Deepika, Y. R. Lim, I. W. Nah, K.-R. Lee, L. A. Archer and W. Il Cho, *Nature Energy*, 2018, **3**, 889-898.
37. S. Jiao, X. Ren, R. Cao, M. H. Engelhard, Y. Liu, D. Hu, D. Mei, J. Zheng, W. Zhao, Q. Li, N. Liu, B. D. Adams, C. Ma, J. Liu, J.-G. Zhang and W. Xu, *Nature Energy*, 2018, DOI: 10.1038/s41560-018-0199-8.
38. M. N. Obrovac and V. L. Chevrier, *Chemical Reviews*, 2014, **114**, 11444-11502.
39. G. L. Henriksen and D. R. Vissers, *Journal of Power Sources*, 1994, **51**, 115-128.
40. J. Zhao, G. Zhou, K. Yan, J. Xie, Y. Li, L. Liao, Y. Jin, K. Liu, P.-C. Hsu, J. Wang, H.-M. Cheng and Y. Cui, *Nature Nanotechnology*, 2017, **12**, 993-999.

41. H. Ye, Z. J. Zheng, H. R. Yao, S. C. Liu, T. T. Zuo, X. W. Wu, Y. X. Yin, N. W. Li, J. J. Gu and F. F. Cao, *Angewandte Chemie International Edition*, 2019, **58**, 1094-1099.
42. Z. Chen, L. Christensen and J. R. Dahn, *Electrochemistry Communications*, 2003, **5**, 919-923.
43. J. W. Slotboom and H. C. de Graaff, *Solid-State Electronics*, 1976, **19**, 857-862.
44. T. Jensen, A. Diening, G. Huber and B. H. T. Chai, *Optics Letters*, 1996, **21**, 585-587.
45. A. D. Pelton, *Bulletin of Alloy Phase Diagrams*, 1986, **7**, 223-228.
46. T. Xu, C. Lin, C. Wang, D. L. Brewe, Y. Ito and J. Lu, *Journal of the American Chemical Society*, 2010, **132**, 2151-2153.
47. A. C. Kozen, C.-F. Lin, A. J. Pearse, M. A. Schroeder, X. Han, L. Hu, S.-B. Lee, G. W. Rubloff and M. Noked, *ACS Nano*, 2015, **9**, 5884-5892.
48. K. N. Wood, M. Noked and N. P. Dasgupta, *ACS Energy Letters*, 2017, **2**, 664-672.
49. Y. Cao, M. Li, J. Lu, J. Liu and K. Amine, *Nature Nanotechnology*, 2019, **14**, 200-207.